Theoretical investigation of $CdIn_2S_4$: A possible substitute for CdS in $CuIn_{1-x}Ga_xSe_2$-based photovoltaic devices

Emmanuel V. Péan,[1,2] Nicolas Barreau,[1] Julien Vidal,[3,4] Camille Latouche,[1,*] and Stéphane Jobic[1]

[1]*Institut des Matériaux Jean Rouxel (IMN), Université de Nantes, CNRS, 2 rue de la Houssinière, 44322 Nantes, France*

[2]*SPECIFIC, College of Engineering, Swansea University, Bay Campus, Fabian Way, Crymlyn Burrows, Swansea, SA1 8EN, United Kingdom*

[3]*Department EFESE, EDF R&D, 6 quai Watier, 78401 Chatou, France*

[4]*Institute for Research and Development of Photovoltaic Energy (IRDEP), UMR 7174 CNRS/EDF R&D/Chimie ParisTech-PSL, 6 quai Watier, 78401 Chatou, France*

(Received 18 July 2017; revised manuscript received 19 October 2017; published 28 November 2017)

Herein we report a theoretical investigation based on density-functional theory (DFT) calculations devoted to the nature of charge carriers in $CdIn_2S_4$. Our simulations led to unambiguous results concerning the origin of *n*-type semiconductivity and its magnitude in this material. Namely, the calculated defect formation energies demonstrate that the cadmium substoichiometry is more favorable than the indium one to account for *n*-type conductivity. Moreover, the anionic vacancies would not be the driving force of the occurring processes but a sulfur-poor atmosphere has to be privileged compared to a sulfur-rich one to favor the formation of $CdIn_2S_4$ with understoichiometry in Cd(II) and thus achieve a higher concentration of free electrons at room temperature.

DOI: 10.1103/PhysRevMaterials.1.064605

I. INTRODUCTION

The $CdIn_2S_4$ material has met a renewed interest these last few years since it has been identified at the $Cu(In,Ga)Se_2/CdS$ interface in high-efficiency CIGSe thin-film solar cells [1,2]. Following this first observation, $Cu(In,Ga)Se_2/CdIn_2S_4$ heterojunctions were then fabricated by the coevaporation technique and the related solar cells demonstrated 16.2% efficiency [3], which makes this material a promising candidate to substitute CBD (deposited by chemical bath) CdS as a buffer layer in CIGSe thin-film solar-cell technology [4]. For two decades now, the champion devices have been fabricated from polycrystalline *p*-$Cu(In,Ga)Se_2$ absorber layer deposited following a vacuum-based process, either coevaporation or rapid thermal treatment of stacked-elemental layers [5]. To date, *n*-CdS CBD is the only junction partner to *p*-CIGSe allowing the achievement of conversion efficiency close to 23% [6,7]. Nevertheless, such a wet deposition technique implies additional fabrication costs because of chemicals storage and recycling, which assuredly slow the large-scale production of panels down. The model we recently proposed to explain the beneficial influence of heavy alkali fluoride postdeposition treatment (i.e., KF-PDT) implies the formation of an ultrathin (5-nm-thick) $CdIn_2S_4$ layer at the CIGSe/CdS interface during the (CBD) CdS deposition [1]. We recently reported on the synthesis of this $CdIn_2S_4$ material as thin film by coevaporation on glass substrates; this successful approach gave us the opportunity to determine the physicochemical and optoelectronic properties of this interface layer. However, to further explore the correlations between the synthesis conditions and the material properties for the targeted applications, it appeared necessary to theoretically investigate the influence of crystal point defects on the optoelectronic characteristics of this alternative buffer layer. Calculations were thus initiated to get insight on the nature of defects in the $CdIn_2S_4$ spinel structure type and to shed light on the origin of its *n*-type character, which is required for the targeted photovoltaic application.

II. COMPUTATIONAL DETAILS

Optimizations were performed using the General Gradient Approximation (GGA)-PBE functional [8] and VASP software [9–11]. The perfect cubic structure of the direct spinel $CdIn_2S_4$ material constituted of 56 atoms was refined using a 600-eV cutoff energy. s^2d [10], s^2p^1d [10], and s^2p [4] valence electrons were considered for Cd, In, and S atoms, respectively, together with the projected augmented-wave treatment. Band occupations and density of states were calculated in a $3\times3\times3$ Γ-centered Monkhorst-Pack *k*-points grid using the tetrahedron method. Due to the severe underestimation of the band gap using such method, GW calculations were performed on top of the GGA-optimized perfect cell. To investigate the defected cells, the optimized cell parameters of the host cell were kept constant and only internal atomic positions were relaxed. Formation energies plot, densities of state, and band structure were depicted using the PYDEF program [12].

The following equation was used to calculate the defect formation energy in different charge states:

$$E_{\text{for}}^{D,q}(\Delta E_F) = E_{\text{tot}}^{D,q} - E_{\text{tot}}^{H} + \sum_i n_i\left(\mu_i^{\circ} + \Delta\mu\right) + q\left(E_V^H + \Delta E_F\right) + \text{corr}(\alpha,q). \quad (1)$$

Here, $E_{\text{for}}^{D,q}$ is the formation energy of the defect D in the state of charge q (at $T = 0\,\text{K}$). It depends on the total energies of the defect and the host structures ($E_{\text{tot}}^{D,q}$ and E_{tot}^{H}, respectively). The $n_i(\mu_i^{\circ} + \Delta\mu)$ terms represent the global contribution to the chemical potentials of the species involved in the defect and can be associated with the synthesis conditions. More precisely, n_i corresponds to the number of atoms added ($n_i < 0$) or removed ($n_i > 0$), μ_i° is the chemical potential of reference, computed from the stable phases of the species (i.e., elemental Cd, In, and α-S_8), and $\Delta\mu$ is the variation of

*camille.latouche@univ-cnrs-imn.fr

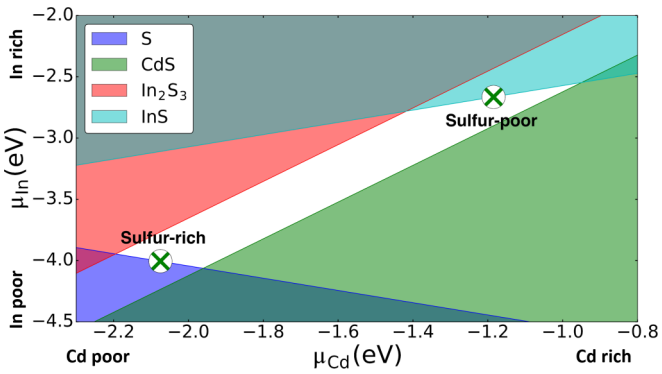

FIG. 1. Chemical potentials determination diagram (at $T = 0$ K). Each colored zone represents forbidden values for $CdIn_2S_4$.

this potential depending on the stability domain of the material (Fig. 1).

The calculated stability domain at $T = 0$ K of the material is depicted in Fig. 1. All the colored areas correspond to conditions in which another material is more likely to be formed (e.g., InS, In_2S_3, CdS, S). As a consequence, $CdIn_2S_4$ can solely be obtained in the white area. As a matter of fact, the control of sulfur atmosphere is not obvious and may be difficult. Therefore, it has been chosen to study the potential impact of the intrinsic defects on the electronic structure of the $CdIn_2S_4$ material prepared in both S-rich and S-poor conditions. The value of the chemical potentials might be estimated using different corrective schemes. The values obtained in our study for In, Cd, and S are listed in Table I [13].

Finally, $q(E_V^H + \Delta E_F)$ corresponds to the electronic reservoir energy where E_V^H is the valence-band maximum (VBM) energy of the host structure obtained at the DFT level of theory and ΔE_F corresponds to the variation of the Fermi level with respect to the VBM.

A. Potential alignment

One of the main drawbacks of the defect formation energy calculations is coming from the fact that we are using a finite (super)cell formalism to simulate an infinite system where simple or complex defects (neutral or charged) are randomly distributed and well separated from each other. This leads to many corrections to apply to account for realistic predictions.

TABLE I. Chemical potential of the different atomic species depending on the synthesis conditions.

Atmosphere	S-poor	S-rich
	$\Delta\mu$(eV)	
Cd	−0.49	−1.38
In	−0.17	−1.50
S	−0.89	0.00
	μ(eV) ($\mu^\circ + \Delta\mu$)	
Cd	−1.19	−2.08
In	−2.67	−4.00
S	−5.01	−4.12

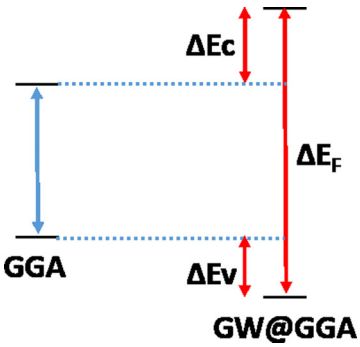

FIG. 2. ΔE_c and ΔE_v corrections.

In particular, when a net charge (q) is introduced, the charged system depends on an undetermined shift of the energy levels (the so-called potential alignment, PA). As a matter of fact, it becomes mandatory to align the VBM in the calculations of (charged) defects with respect to the host cell to get back the validity of the formation energy calculations. To express this PA, it is important to investigate the potential felt by an atom in the defect structure ($V^r_{D,q}$) and to compare this result to the one felt in the host cell (V^r_{host}) without defect such as

$$\Delta V = V^r_{D,q} - V^r_{\text{host}}. \tag{2}$$

As the PA is an averaged value of the potential felt by atoms beyond a reasonable distance from the defect [14,15], the potential alignment is then written as

$$\Delta E_{PA} = q \times \overline{\Delta V}. \tag{3}$$

B. Edge position corrections

At the GGA level of accuracy, the obtained band gap is strongly underestimated. One of the most popular solutions in the defect community has been to use the so-called scissor operator such that the band gap obtained is in good agreement with experimental values [16–32]. In the present paper, many-body perturbation theory has been considered to correct the band gap, which was found to be of high accuracy for a very large class of materials [33]. In such case, a simple way to correct the underestimated GGA band gap, e.g., the band edges, is to perform a GW-type calculation on the relaxed GGA structure. The corrections are labeled ΔE_c and ΔE_v, respectively, for the conduction band (CB) and for the valence band (VB) (Fig. 2). This leads to the following correction of the defect formation energy [34]:

$$q \times \Delta E_V. \tag{4}$$

In the case of $CdIn_2S_4$, $\Delta E_V = -0.27$ eV and $\Delta E_C = 1.1$ eV were found.

C. Image charge correction

Corrections for electrostatic interaction which correspond to spurious interaction between defects sitting in neighboring cells take properly into account a Madelung-like term and a quadripolar term. In the present paper, the Lany and Zunger

[14] compact form has been used:

$$\Delta E_{MP} = (1 + c_{sh}[1 - \epsilon^{-1}])\frac{q^2\alpha_M}{2\epsilon V^{1/3}}, \quad (5)$$

in which α_M is the Madelung constant, ϵ is the dielectric constant of the material, and V is the (super)cell volume. The c_{sh} term depends on the cell geometry and usually has a value between around -0.35 and -0.5 for the standard cell symmetries (bcc, fcc, sc) [14]. It should also be mentioned that different electrostatic corrections might be applied [35,36].

D. Moss-Burstein-type band filling

In the case of shallow defects, it is important to correctly render the band-filling correction effects. Indeed, when defect-related electronic states lie above or below the conduction band minimum (CBM) and the valence band maximum, respectively, the electron (holes) occupying this state relax to the perturbated host state (PHS), resulting in a Moss-Burstein-like effect for small sizes of supercell. The corrections are therefore included in order to eliminate the band-filling effects for shallow donors (acceptors). This correction is of capital importance because calculations herein are carried out with a defect density of about $7.5 \times 10^{20}/\mathrm{cm}^3$, while a density of about $10^{17}-10^{19}$ defects/cm^3 is expected in real crystals (difference of several orders of magnitude).

For electrons in the conduction band, the correction is

$$\Delta E_{MB}^{e^-} = -\sum^{n,k} \omega_k \eta_{n,k}\left(\epsilon_{n,k} - \left[E_C^{\mathrm{host}} + \overline{\Delta V}\right]\right) \cdot \Theta\left(\epsilon_{n,k} - \left[E_C^{\mathrm{host}} + \overline{\Delta V}\right]\right), \quad (6)$$

where ω_k is the weight of k-point k, $\eta_{n,k}$ of the occupation of band n for k-point k, $\epsilon_{n,k}$ is the energy of band n for k-point k, and Θ is the Heaviside function. Similarly, for holes in the valence band,

$$\Delta E_{MB}^{\mathrm{holes}} = -\sum^{n,k} \omega_k\left(2 - \eta_{n,k}\right)\left(\left[E_V^{\mathrm{host}} + \overline{\Delta V}\right] - \epsilon_{n,k}\right) \cdot \Theta\left(\left[E_V^{\mathrm{host}} + \overline{\Delta V}\right] - \epsilon_{n,k}\right). \quad (7)$$

In the case of $CdIn_2S_4$, the Moss-Burstein correction of the CB is much higher than for the VB as the CB is highly delocalized (see Supplemental Material [37]).

E. Perturbated host state

Finally, as explained above, when one introduces defects in a cell, it can also create localised states which are named defect localized states (DLS). In the case where a DLS is in the conduction (valence) band, the electrons (holes) which may occupy it will fall down to the CBM (VBM) level where they will occupy a PHS. The correction of the electronic gap leads to the correction of the quasiparticles in these PHSs:

$$\Delta E_{\mathrm{PHS}} = +z_e\Delta E_C - z_h\Delta E_V, \quad (8)$$

where z_e electrons are located in the conduction band and z_h holes are in the valence band.

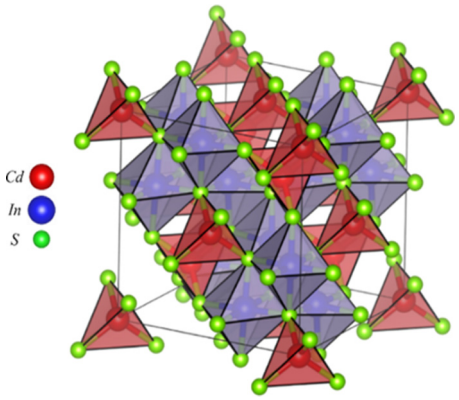

FIG. 3. $CdIn_2S_4$ direct spinel structure.

F. Defect transition-energy level

The defect transition-energy levels $\epsilon(q/q')$ are defined as the values of the Fermi level for which the formation energy of a charge state q is equal to the formation energy of a charge state q'. As a consequence, the $\epsilon(q/q')$ formalism indicates the transition level where the defect in the charge state q is the most stable while for higher or lower values of ΔE_F the charge state q' becomes the most stable, and follows the below equation:

$$\epsilon(q/q') = \frac{E_{\mathrm{for}}^{D,q'}(0) - E_{\mathrm{for}}^{D,q}(0)}{q - q'}. \quad (9)$$

To some extent, this $\epsilon(q/q')$ transition energy level may be regarded as a border where the q and q' charge states of the defect under focus are in identical concentration, as pK_a in acid/base reactions that corresponds to a specific pH at which concentrations of acid and base are the same. For ΔE_F, or for an overall given redox potential associated with $\epsilon(q/q')$, the probability to stabilize the charge defect q is rigorously equal to the one to stabilize the charge defect q'. These transition levels are commonly sketched with a schematic electronic structure to explain transport properties (i.e., positioning of the acceptor and donor levels).

III. RESULTS AND DISCUSSION

A. Perfect cell

We first discuss the ideal $CdIn_2S_4$ structure. The $CdIn_2S_4$ material can be described as direct spinel, i.e., a cubic cell ($Fd-3m$) built upon a closed packing of S^{2-} anions where only one-eighth of tetrahedra and one-half of octahedra are occupied by Cd^{2+} and In^{3+} cations, respectively. According to our simulations, the optimized cell parameter is 11.02 Å and fits nicely with the reported ones in the literature (around 10.85 Å) (Fig. 3).

However, despite a good structural description including atom positions and cell parameters [38,39], the calculated band gap in GGA is strongly underestimated with respect to the experimental one (1.05 vs 2.40 eV, indirect) but is sufficient to describe the electronic structure. According to the density of states (Fig. 4), the VBM is mainly localized on the sulfur atoms whereas the CBM is strongly constituted by the cations and especially by indium. The dielectric constants have been

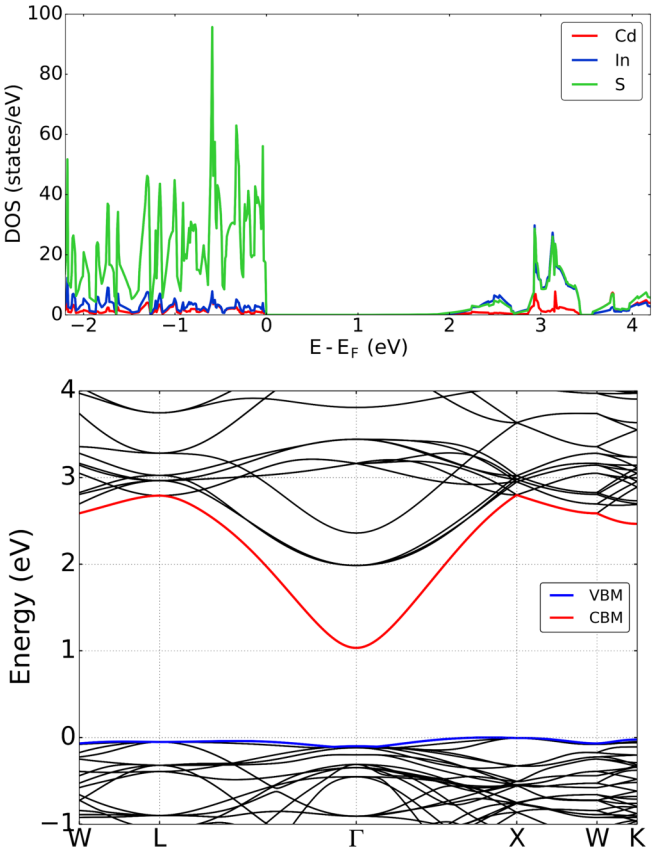

FIG. 4. Density of states vs energy and band-dispersion diagram of a hypothetical perfect $CdIn_2S_4$ material.

computed at this level of accuracy. The computed ε_e (also labeled ε_∞, the high-frequency dielectric constant) and ε_0 (the static dielectric constant) are in reasonable agreement with respect to the experimental ones (respectively, 7.4 vs 6.5 [40] and 14.3 vs 17.3 [41]). Such a large dielectric constant coupled with the large band gap will tend to screen the electrostatic interactions and yield low-value image-charge corrections. The correction of the band gap has been performed on the relaxed GGA structure, using the GW ansatz. In this case, the calculated band gap is 2.39 eV and fits perfectly the experimental one (∼2.40 eV, indirect band gap) [3] with no striking changes on the density of states. The direct band gap is estimated at 2.70 eV [3].

Moreover, the band diagram (GGA) demonstrates a rather flat valence profile with high hole effective mass (m_h^*) while the conduction band displays a very dispersive nature with low electron effective mass (m_e^*). The latter will induce large band-filling effect correction in the case of shallow donor defects. This fact suggests that photopromoted electrons would exhibit a significant mobility in contrast to remaining holes.

On these grounds, it becomes natural to make the hypothesis that the semiconductor activity of the material is not coming from an intrinsic charge transfer but due to the presence of defects. Therefore, a thorough first-principles calculations investigation has been performed. In the following section, the formation energy and the contributions of simple point defects (vacancies, interstitial, and antisites) are discussed. In the second section, complexes point defects are discussed.

B. Simple defects

The following defects have been investigated: V_S, V_{In}, V_{Cd}, Cd_i, In_i, Cd_{In}, and In_{Cd} with different charge states (e.g., for sulfur vacancy: V_S^{+2}, V_S^{+}, V_S^{0}; substitution of one cadmium by one indium: In_{Cd}^{+}, In_{Cd}^{0}). The state of charge of the defect can be understood through the electronic count. The perfect bulk structure is computed with a total of 496 valence electrons. By removing of sulfur atom, creating a sulfur vacancy, 6 valence electrons have been removed from the system, leading to 490 electrons left in the cell and the defect is considered neutral (V_S^0). To take into account the ionization of the defect, a vacancy in this example, the total electron number is modified. If two extra electrons are removed, leading to a total valence electron number of 488, it is the equivalent to the removal of S^{2-} and the defect is charged $2+$ (V_S^{2+}). Moreover, in the case of the aforementioned substitution (In_{Cd}), the neutral defect corresponds to In_{Cd}^0 and the total electron count is now 497. This type of substitution is supposed to lead to a positively charged defect. This is the case when the defect is ionized once, the total electron number is thus 496, and the defect is In_{Cd}^+. To be coherent with the most plausible synthesis atmospheres, the limiting S-rich and S-poor conditions have been studied. The defects corresponding to vacancies are first discussed. V_{In} possesses different $\epsilon(q/q')$ transition levels between $+0.5$ and $+1.25$ eV together with high formation energies (around 4 eV at low ΔE_F) for both conditions. V_{Cd} exhibits the same trend but this time the formation energies slightly decrease to 2 and 3 eV in S-poor and S-rich atmospheres, respectively. Both cationic vacancies lead to neither p- nor n- type conduction at room temperature due to transition levels located far from the VBM and the CBM. Furthermore, the formation energies are too high, which will result in very low concentration of such defect in the material (*vide infra*). Sulfur vacancy follows a negative U behavior, i.e., only the neutral and $+2$ charge state are stable [42]. Moreover, the $\epsilon(+2/0)$ transition level appears around 1.7 eV with respect to the VBM in the band gap, quite far from the CBM, and with formation energy near 2 eV. The spinel structure type possesses a high capability to accept the insertion cations, therefore the Cd_i and In_i defects have been investigated. First, one should notice that for both defects, the transition level $\epsilon(+1/0)$ appears close to the CBM. Therefore, these positions in the band gap make these defects a serious candidate for n-type doping. However, the formation energy of the Cd_i defect is very high and is thus inaccessible. Furthermore, in the S-rich atmosphere, both defects possess an important formation energy which could prevent its accessibility. Finally, in the S-poor condition, it must be pointed out that the insertion of indium in interstitial environment seems more possible due to its lower formation energy. However, due to the relative high energy, it should not play a significant role in the observed properties of the material. The substitutions of a cation by another one, i.e., In_{Cd} and Cd_{In}, have also been investigated. In the case of Cd_{In}, as a +II cation replaces a +III one, the defect would lead to a possible p-type doping. Despite a low defect formation energy, the transition level is quite far from the VBM, making such defect an inefficient p-type dopant. On the contrary, according to our simulations at this level of accuracy, the In_{Cd} defect possesses an $\epsilon(+1/0)$ transition located at the bottom

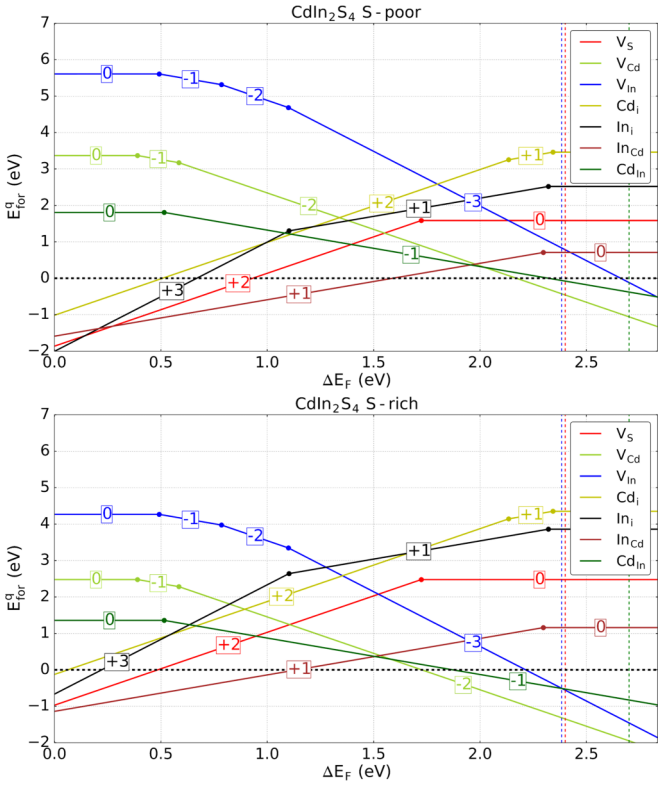

FIG. 5. Defect formation energy vs Fermi level in $CdIn_2S_4$ prepared in S-poor and S-rich conditions.

of the CBM. Furthermore, this defect is also very plausible to be formed thanks to a low formation energy (∼1 eV), especially in S-poor conditions. All these data are furnished in Fig. 5.

Based on our results of the defect formation energy in Fig. 5, the intrinsic n-type conductivity is favored through an overstoichiometry in In with respect to Cd. The p-type conductivity seems very difficult to achieve for the $CdIn_2S_4$ material because of the positioning of the defect levels which are far from the VBM. The sulfur atmospheres play a critical role concerning the value of the formation energy.

Finally, the domain of Fermi level accessible via doping has to be investigated. As stated before, the p-type semiconductor seems difficult to access while n type is the native conductivity. To estimate this capability, it is necessary to calculate the limit of n-type doping. This limit is achieved when the line (defect) crosses the zero-energy (E^q_{for}) with a negatively charged defect [43]. In our simulations, this limit corresponds to the point where the $V_{Cd}(q = -2)$ crosses the zero-energy line. The values in the band gap are 1.7 and 2.2 eV with respect to the VBM, respectively, for S-rich and S-poor atmospheres. According to our level of accuracy, the n-type limit in the S-poor condition is very close to the CBM and below the hypothetical transition levels leading to this conductivity. This result clearly points at the potential of obtaining intrinsic n type. In contrast, in the S-rich condition, we may speculate that any attempts to obtain significant n-type conductivity in $CdIn_2S_4$ in ambient conditions would be doomed to failure due to the barrier in the dopability domain created by V_{Cd}. (Figure 6).

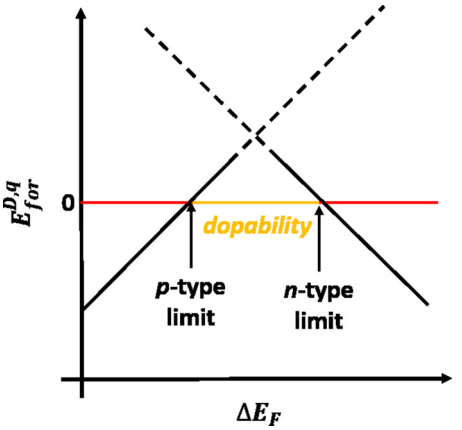

FIG. 6. Limits of the dopability domain in a semiconductor.

C. Complex defects

As the $CdIn_2S_4$ crystallizes as direct spinel structure, it is possible to obtain multiple defects in the cell. Based on the electrostatic interaction between defects, the most probable ones are V_S&V_{Cd}, V_S&V_{In}, Cd_{In}&In_{Cd}, V_S&Cd_{In}, V_{Cd}&In_{Cd} pairs. Therefore, the investigation of complex defects has been started and the associated defect formation energies are provided in Fig. 7.

First, as one can see, the most stable defect is when one cadmium atom and one indium atom have their positions exchanged (Cd_{In}&In_{Cd}). On the one hand, it is important to mention that no transition level is located just below the

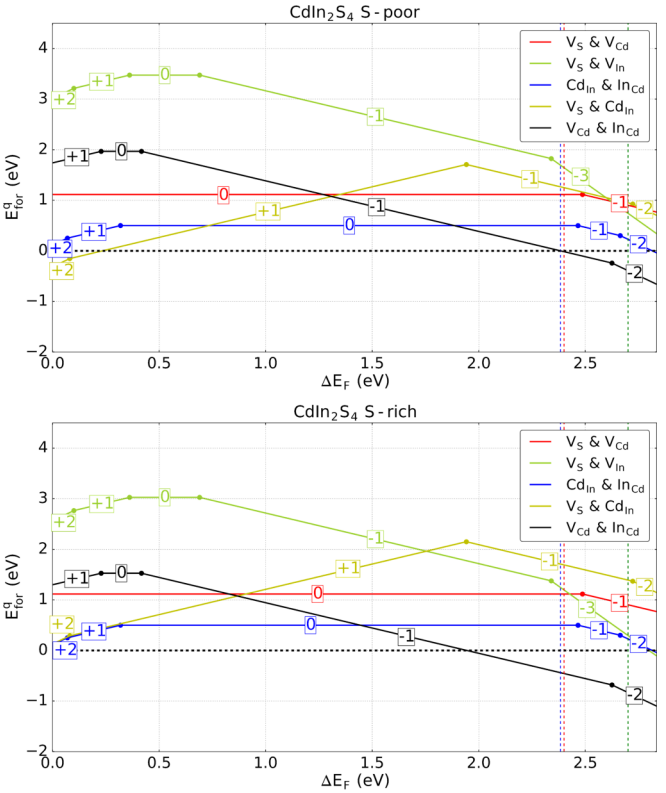

FIG. 7. Defect formation energy of complex defects vs Fermi level in $CdIn_2S_4$ prepared in S-poor and S-rich conditions.

CBM, meaning that this defect is not supposed to give n-type semiconductor. Second, it should be mentioned that in the S-rich atmosphere a transition energy level is present with a formation energy lower than 0.5 eV which is really close to the VBM. However, this defect is hardly expected to be active due to the presence of In_{Cd} defects whose formation energy is null at 1.3 eV in the band gap which annihilates the contribution of this defect. According to results obtained in the simulations, the other complex defects do not interact directly with the properties of the material.

D. Defect concentration of simple defects

The defect concentration $n_{D,q}(E_F)$ of a defect D in charge state q can be approximated using the following equation [44]:

$$n_{D,q}(E_F) \approx N \cdot \exp\left(\frac{-E_{\text{for}}^{D,q}(E_F)}{k_B T}\right), \tag{10}$$

where k_B is the Boltzmann constant, N is the number of sites available to the defect, T is the synthesis temperature (400 °C), and E_F ($E_F = E_V + \Delta E_F$) is the Fermi energy. In that context, entropic terms are neglected because they are considered minor compared to the enthalpy terms. The value of the Fermi energy is then determined by solving iteratively the charge-neutrality equation

$$-n_e(E_F) + n_h(E_F) + \sum_D q_D \cdot n_{D,q_D}(E_F) = 0. \tag{11}$$

Here $n_e(E_F)$ and $n_h(E_F)$ are, respectively, the concentrations of free electrons and holes for a Fermi energy at a given temperature.

$$n_e(E_F) = \int_{E_C}^{+\infty} g_e(E) \cdot f_{FD}(E - E_F) \cdot dE \tag{12}$$

and

$$n_h(E_F) = \int_{-\infty}^{E_V} g_h(E) \cdot (1 - f_{FD}(E - E_F)) \cdot dE, \tag{13}$$

where $f_{FD}(E - E_F)$ is the Fermi-Dirac function:

$$f_{FD}(E - E_F) = \frac{1}{1 + \exp\left(\frac{E - E_F}{k_B T}\right)}, \tag{14}$$

and $g_e(E)$ and $g_h(E)$ are, respectively, the density of states of electrons and holes in 3D:

$$g_{e,h}(E) = \frac{1}{4\pi^2}\left(\frac{2m_{e,h}^*}{\hbar^2}\right)^{3/2}\sqrt{E}. \tag{15}$$

The electron and hole effective masses (m_e^* and m_h^*) were calculated by fitting the CBM and the VBM of the band-structure diagram of the hypothetical perfect structure material using the parabolic relation $E(\boldsymbol{k}) = \frac{\hbar^2}{2m^*}\boldsymbol{k}^2$ ($m_e^* = 0.044\ m_e$ and $m_h^* = 1.065\ m_e$, with m_e the free electron mass). In that framework, ΔE_F values of 1.93 and 1.48 eV (i.e., values consistent with the dopability domain) were calculated for S-poor and S-rich conditions at 400 °C, respectively. The corresponding calculated defect concentrations n_{D,q_D} are gathered in Table II.

TABLE II. Defect concentrations in $CdIn_2S_4$ synthetized at 400 °C in S-rich and S-poor conditions ($E_F = 1.48$ and 1.93 eV, respectively).[a]

	S-rich		S-poor	
	n_D (10^{18}cm^{-3})	q	n_D (10^{18}cm^{-3})	q
V_S	∼0	2	∼0	0
V_{Cd}	∼1.3	−2	∼1.5	−2
V_{In}	∼0	−3	∼0	−3
Cd_i	∼0	2	∼0	2
In_i	∼0	1	∼0	1
In_{Cd}	∼16.6	1	∼16.8	1
Cd_{In}	∼14.1	−1	∼13.9	−1

[a] $N = 32$, 8, 16, 56, 16, 8, and 16 for V_S, V_{Cd}, V_{In}, Cd_i, In_i, In_{Cd}, and Cd_{In}, respectively.

As expected, In_{Cd} and Cd_{In}, and V_{Cd} to a lesser extent, are the dominant point defects in this material. In fact, they almost compensate each other such that the expected induced net doping is very low. Based on defect concentrations calculated at the synthesis temperature, the Fermi levels at room temperature in S-rich and S-poor conditions were determined as well as the free electron concentrations in ambient conditions (the calculated free hole concentrations are almost null in the present case, $n_h \sim 0$ cm^{-3}). As expected for an n-type semiconductor [45,46], the Fermi level significantly rises up when temperature decreases (in relation with a continuous shift from an intrinsic region to a freeze-out region). Hence, in the S-rich case, the Fermi level turns out to be located at −0.38 eV below the conduction band with n_e of $\sim 14 \times 10^{10}$cm^{-3}. In the S-poor case, the Fermi level is located a little higher in energy, i.e., at −0.18 eV below the CBM, and the free electrons concentration increased up to $\sim 3 \times 10^{14}$cm^{-3}. $CdIn_2S_4$ presents thus a natural n-type doping with the highest conductivity achieved under S-poor conditions.

IV. CONCLUSION AND PERSPECTIVES

In the present paper, theoretical calculations have provided insights on the electronic structure of the $CdIn_2S_4$ material. First, the formation energy of multiple simple defects has been investigated in accordance with their state of charges. Second, it has been established unambiguously, according to the level of accuracy used, that the sulfur atmosphere may play a critical role on the performance of $CdIn_2S_4$. Third, according to our calculations, the defects cannot provide p-type conductivity. Fourth, it has been demonstrated that the n type is possible thanks to the incorporation of three defects: In_i, Cd_i, In_{Cd}. The Cd_i defect possesses a too-high formation energy and seems impossible to be formed. In_i defects require less energy than Cd_i but higher than In_{Cd} ones, with a donor level a little deeper than the two previous ones.

ACKNOWLEDGMENTS

This research used resources of CCIPL (Centre de Calcul Intensif des Pays de Loire). The authors greatly acknowledge Ludovic Arzel, Maite Caldes, Catherine Guillot-Deudon, Sylvie Harel, and Alain Lafond for fruitful discussions.

[1] T. Lepetit, S. Harel, L. Arzel, G. Ouvrard, and N. Barreau, IEEE J. Photovoltaics **6**, 1316 (2016).

[2] N. Nicoara, T. Lepetit, L. Arzel, S. Harel, N. Barreau, and S. Sadewasser, Sci. Rep. **7**, 41361 (2017).

[3] N. Barreau *et al.*, Solar RRL (2017), doi:10.1002/solr.201700140.

[4] T. Lepetit, Ph.D. thesis, Université de Nantes, 2015.

[5] S. Niki, M. Contreras, I. Repins, M. Powalla, K. Kushiya, S. Ishizuka, and K. Matsubara, Prog. Photovoltaics Res. Appl. **18**, 453 (2010).

[6] P. Jackson, R. Wuerz, D. Hariskos, E. Lotter, W. Witte, and M. Powalla, Phys. Status Solidi RRL **10**, 583 (2016).

[7] N. Naghavi, D. Abou-Ras, N. Allsop, N. Barreau, S. Bücheler, A. Ennaoui, C.-H. Fischer, C. Guillen, D. Hariskos, J. Herrero, R. Klenk, K. Kushiya, D. Lincot, R. Menner, T. Nakada, C. Platzer-Björkman, S. Spiering, A. N. Tiwari, and T. Törndahl, Prog. Photovoltaics Res. Appl. **18**, 411 (2010).

[8] J. P. Perdew, K. Burke, and M. Ernzerhof, Phys. Rev. Lett. **77**, 3865 (1996).

[9] G. Kresse and J. Furthmüller, Phys. Rev. B **54**, 11169 (1996).

[10] G. Kresse and J. Furthmüller, Comput. Mater. Sci. **6**, 15 (1996).

[11] G. Kresse and D. Joubert, Phys. Rev. B **59**, 1758 (1999).

[12] E. Péan, J. Vidal, S. Jobic, and C. Latouche, Chem. Phys. Lett. **671**, 124 (2017).

[13] V. Stevanović, S. Lany, X. Zhang, and A. Zunger, Phys. Rev. B **85**, 115104 (2012).

[14] S. Lany and A. Zunger, Model. Simul. Mater. Sci. Eng. **17**, 84002 (2009).

[15] Y. Kumagai and F. Oba, Phys. Rev. B **89**, 195205 (2014).

[16] P. M. Beaujuge and J. M. J. Fréchet, J. Am. Chem. Soc. **133**, 20009 (2011).

[17] J. Heyd and G. E. Scuseria, J. Chem. Phys. **121**, 1187 (2004).

[18] W. Tao, G. Qing, L. Yan, and S. Kuang, Chin. Phys. B **21**, 67301 (2012).

[19] F. Karlický, R. Zbořil, and M. Otyepka, J. Chem. Phys. **137**, 34709 (2012).

[20] J. Dai and X. C. Zeng, J. Phys. Chem. Lett. **5**, 1289 (2014).

[21] N. Kharche and S. K. Nayak, Nano Lett. **11**, 5274 (2011).

[22] J. M. Azpiroz, J. M. Ugalde, and I. Infante, J. Chem. Theory Comput. **10**, 76 (2014).

[23] A. Kay, I. Cesar, and M. Grätzel, J. Am. Chem. Soc. **128**, 15714 (2006).

[24] K. Takei, S. Chuang, H. Fang, R. Kapadia, C.-H. Liu, J. Nah, H. S. Kim, E. Plis, S. Krishna, and Y.-L. Chueh, Appl. Phys. Lett. **99**, 103507 (2011).

[25] J. Heyd, J. E. Peralta, G. E. Scuseria, and R. L. Martin, J. Chem. Phys. **123**, 174101 (2005).

[26] A. Alkauskas and A. Pasquarello, Phys. Rev. B **84**, 125206 (2011).

[27] P. Liao and E. A. Carter, Phys. Chem. Chem. Phys. **13**, 15189 (2011).

[28] S. Tongay, J. Zhou, C. Ataca, K. Lo, T. S. Matthews, J. Li, J. C. Grossman, and J. Wu, Nano Lett. **12**, 5576 (2012).

[29] P. García-Fernández, S. Ghosh, N. J. English, and J. A. Aramburu, Phys. Rev. B **86**, 144107 (2012).

[30] J.-W. Song, K. Yamashita, and K. Hirao, J. Chem. Phys. **135**, 71103 (2011).

[31] S. Grimme, J. Comput. Chem. **27**, 1787 (2006).

[32] F. Bruneval and M. A. L. Marques, J. Chem. Theory Comput. **9**, 324 (2012).

[33] H. Peng, D. O. Scanlon, V. Stevanovic, J. Vidal, G. W. Watson, and S. Lany, Phys. Rev. B **88**, 115201 (2013).

[34] S. Lany and A. Zunger, Phys. Rev. B **78**, 235104 (2008).

[35] C. Freysoldt, J. Neugebauer, and C. G. Van de Walle, Phys. Rev. Lett. **102**, 016402 (2009).

[36] H.-P. Komsa, T. T. Rantala, and A. Pasquarello, Phys. Rev. B **86**, 045112 (2012).

[37] See Supplemental Material at http://link.aps.org/supplemental/10.1103/PhysRevMaterials.1.064605 for calculation protocol including tags used.

[38] Y. Seminovski, P. Palacios, P. Wahnón, and R. Grau-Crespo, Appl. Phys. Lett. **100**, 102112 (2012).

[39] V. Krasnenko and M. G. Brik, Mater. Res. Express **1**, 15905 (2014).

[40] H. Neumann, W. Kissinger, F. Levy, H. Sobotta, and V. Riede, Cryst. Res. Technol. **24**, 1165 (1989).

[41] N. N. Syrbu, S. I. Radautsan, R. V. Cretu, V. E. Tezlevan, and N. A. Moldoveanu, Cryst. Res. Technol. **31**, 307 (1996).

[42] G. D. Watkins, in *Advances in Solid State Physics*, edited by P. Grosse, Advances in Solid State Physics (Springer, Berlin, Heidelberg, 1984), Vol. 24, pp. 163–189.

[43] A. Zunger, Appl. Phys. Lett. **83**, 57 (2003).

[44] Y. Quéré, *Physique Des Matériaux: Cours et Problèmes* (Ellipses, Paris, 1988).

[45] S. M. Sze and N. K. Kwok, *Physics of Semiconductor Devices*, 3rd ed. (Wiley, Hoboken, NJ, 2006).

[46] R. E. Hummel, *Electronic Properties of Materials* (Springer, New York, 2011).